Inorganic Chemistry

Article

pubs.acs.org/IC

Synthesis, Structure, and Characterization of New $Li^+ - d^0 -$ Lone-Pair $-$ Oxides: Noncentrosymmetric Polar $Li_6(Mo_2O_5)_3(SeO_3)_6$ and Centrosymmetric $Li_2(MO_3)(TeO_3)$ (M = Mo^{6+} or W^{6+})

Sau Doan Nguyen[†] and P. Shiv Halasyamani*[,†]

[†]Department of Chemistry, University of Houston, 136 Fleming Building, Houston, Texas 77204-5003, United States

Supporting Information

ABSTRACT: New quaternary lithium $-$ d^0 cation $-$ lone-pair oxides, $Li_6(Mo_2O_5)_3(SeO_3)_6$ ($Pmn2_1$) and $Li_2(MO_3)(TeO_3)$ ($P2_1/n$) (M = Mo^{6+} or W^{6+}), have been synthesized and characterized. The former is noncentrosymmetric and polar, whereas the latter is centrosymmetric. Their crystal structures exhibit zigzag anionic layers composed of distorted MO_6 and asymmetric AO_3 (A = Se^{4+} or Te^{4+}) polyhedra. The anionic layers stack along a 2-fold screw axis and are separated by Li^+ cations. Powder SHG measurements on $Li_6(Mo_2O_5)_3(SeO_3)_6$ using 1064 nm radiation reveal a SHG efficiency of approximately 170 × α-SiO_2. Particle size vs SHG efficiency measurements indicate $Li_6(Mo_2O_5)_3(SeO_3)_6$ is type 1 nonphase-matchable. Converse piezoelectric measurements result in a d_{33} value of ~28 pm/V and pyroelectric measurements reveal a pyroelectric coefficient of −0.43 $\mu C/m^2K$ at 50 °C for $Li_6(Mo_2O_5)_3(SeO_3)_6$. Frequency-dependent polarization measurements confirm that $Li_6(Mo_2O_5)_3(SeO_3)_6$ is nonferroelectric, i.e., the macroscopic polarization is not reversible, or 'switchable'. Infrared, UV−vis, thermogravimetric, and differential thermal analysis measurements and electron localization function calculations were also done for all materials.

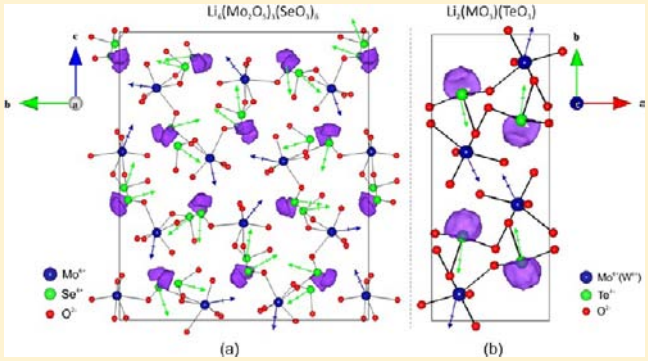

INTRODUCTION

Polar materials have many practical applications in electronic and laser technologies owing to their functional properties such as second-harmonic generation (SHG), piezoelectricity, pyroelectricity, and/or ferroelectricity.[1−4] The search for new polar materials continues to be an active and challenging task for material scientists and solid-state chemists. The structure−property relationships of polar materials have been well studied,[3] yet the understanding of how polar structures are created from structural building units is far from complete. The packing and polarization alignment of structural building units are found to depend on cation sizes, hydrogen bonding, and hard and soft cation−anion interactions. Influence of cation sizes on altering structures from centrosymmetric (CS) to noncentrosymmetric (NCS) has been observed and reported for several systems such as $MNaNbOF_5$ (M =K^+, Cs^+),[5] $A_2Ti(IO_3)_6$ (A = Li^+, Na^+, K^+, Rb^+, Cs^+, and Tl^+),[6] A_2SeMoO_6,[7] (A = Na^+, K^+, Rb^+) $ACuTe_2O_7$,[8] and $A(Mo_2O_5)(SeO_3)_2$ (A= Sr^{2+}, Ba^{2+}, Pb^{2+}).[9] Recently, using hydrogen bonding to direct the alignment of polar lambda structural building units, Donakowski et al. have been able to prepare a new polar material, $CuVOF_4(H_2O)_7$, from CS $MVOF_4(H_2O)_7$ (M = Co^{2+}, Ni^{2+}, and Zn^{2+}).[10] In addition, using hard, Na^+, and soft, Ag^+, cations, Fry et al. have been able to direct the orientation of polar oxyfluoride groups, thereby altering the undoped NCS polar $Na_3WO_3F_3$ (R3) to the doped CS $Na_{1.5}Ag_{1.5}MoO_3F_3$ and $Na_{1.5}Ag_{1.5}WO_3F_3$ ($R\bar{3}$).[11] Despite these successes, the systematic engineering and design of new polar crystal structures remain an ongoing challenge.

The macroscopic polarity in materials emanates from the local polarity of building blocks of the structure. Chen's group proposed using acentric π-conjugated systems, particularly planar borate rings, to enhance nonlinear optical responses and to direct new noncentrosymmetric (NCS) borate-based materials.[12−15] Recently, Zou et al. have successfully reported a new series of polar alkaline−alkaline earth fluoride carbonates with strong SHG efficiencies based on π-conjugated CO_3^{2-} anionic groups.[16] Poeppelmeier et al. have successfully used oxyfluoride groups to create new polar materials,[5,10,17−23] whereas cations that are susceptible to second-order Jahn−Teller (SOJT) distortions[24−30] have been successfully employed in preparing many new polar materials in our group as well as others.[6,7,31−36]

With respect to lithium compounds containing SOJT cations, only a few materials have been reported, $LiVTeO_5$ ($P2_12_12_1$),[57] $Li(VO_2)_3(TeO_3)_2$ (P-1),[58] $Li(MoO_3)(IO_3)$ ($P2_1$),[59] and $Li_8Bi_2Mo_7O_{28}$ ($I\bar{4}$).[60] Of these only $Li(MoO_3)(IO_3)$ is polar. No lithium compounds containing Mo^{6+} (or W^{6+}) and Se^{4+} (or Te^{4+}) have been reported to date even though many polar compounds have been published that contain these SOJT cations and other alkali cations such as $Na_2Te_3Mo_3O_{12}$,[36] $R_2(MO_3)_3(AO_3)$ (R = Rb^+, Cs^+; M = Mo^{6+}, W^{6+}; A = Se^{4+},

Received: June 22, 2012
Published: August 23, 2012

   dx.doi.org/10.1021/ic301334c | Inorg. Chem. 2012, 51, 9529−9538

Te^{4+}).[34,44,61−64] In this paper, we report on the synthesis and characterization of new lithium − d^0 cation − lone-pair compounds, NCS polar $Li_6(Mo_2O_5)_3(SeO_3)_6$ and CS $Li_2(MO_3)(TeO_3)$ (M = Mo^{6+} or W^{6+}). In addition to the crystal structures, UV−vis and IR spectroscopy and thermal analyses for all reported materials as well as SHG, piezoelectricity, and polarization measurements for $Li_6(Mo_2O_5)_3(SeO_3)_6$ are also reported.

EXPERIMENTAL DETAILS

Reagents. Li_2MoO_4 (Alfa Aesar, 98.5%), Li_2CO_3 (Alfa Aesar, 99%), SeO_2 (Alfa Aesar, 99.4%), TeO_2 (GFS, 99.6%), and WO_3 (Alfa Aesar, 99.8%) were used as received.

Synthesis. Crystals of $Li_6(Mo_2O_5)_3(SeO_3)_6$ were prepared by solid state techniques. A mixture of 0.174 g (1.00×10^{-3} mol) of Li_2MoO_4 and 0.110 g (1.00×10^{-3} mol) of SeO_2 was thoroughly ground and pressed into a pellet. The pellet was placed in a Pyrex tube that was evacuated and flame-sealed. The sealed ampule was heated to 300 °C for 12 h and then 450 °C for 24 h and finally cooled to room temperature at 6 °C h^{-1}. The resultant pellet was washed with distilled water and revealed only colorless rod-shaped crystals (80% yield based on SeO_2). Bulk $Li_6(Mo_2O_5)_3(SeO_3)_6$ was prepared by combining 0.174 g (1.00×10^{-3} mol) of Li_2MoO_4, 0.220 g (2.00×10^{-3} mol) of SeO_2, and 0.144 g (1.00×10^{-3} mol) of MoO_3. The mixture was finely ground and pressed into a pellet. The pellet was placed in a Pyrex tube that was evacuated and flame-sealed. The sealed ampule was heated to 400 °C for four days with three intermittent regrindings resulting in single phase $Li_6(Mo_2O_5)_3(SeO_3)_6$ (see Figure S1).

Crystals of $Li_2(MoO_3)(TeO_3)$ and $Li_2(WO_3)(TeO_3)$ were grown using hydrothermal techniques. A mixture of 0.110 g (1.50×10^{-3} mol) of Li_2CO_3, 0.160 g (1.00×10^{-3} mol) of TeO_2, 0.144 g (1.00×10^{-3} mol) of MoO_3 and 3 mL of H_2O for $Li_2(MoO_3)(TeO_3)$ and a mixture of 0.110 g (1.50×10^{-3} mol) of Li_2CO_3, 0.160 g (1.00×10^{-3} mol) of TeO_2, 0.232 g (1.00×10^{-3} mol) of WO_3, and 3 mL of H_2O for $Li_2(WO_3)(TeO_3)$ were placed in separate 23 mL Teflon-lined autoclaves that were subsequently closed. The autoclaves were heated to 230 °C for 4 days and then cooled slowly to room temperature at a rate of 6 °C h^{-1}. The products consisted of only colorless block crystals (~90% yield based on MoO_3 or WO_3).

Bulk phases of $Li_2(MoO_3)(TeO_3)$ and $Li_2(WO_3)(TeO_3)$ were prepared by solid state techniques. A mixture of 0.074 g (1.0×10^{-3} mol) of Li_2CO_3, 0.160 g (1.00×10^{-3} mol) of TeO_2, and 0.144 g (1.00×10^{-3} mol) of MoO_3 for $Li_2(MoO_3)(TeO_3)$ and a mixture of 0.074 g (1.0×10^{-3} mol) of Li_2CO_3, 0.160 g (1.00×10^{-3} mol) of TeO_2, and 0.232 g (1.00×10^{-3} mol) of WO_3 for $Li_2(WO_3)(TeO_3)$ were ground, pressed into pellets, and heated in air to 425 °C for $Li_2(MoO_3)(TeO_3)$ and to 450 °C for $Li_2(WO_3)(TeO_3)$ in three days with two intermittent regrindings to obtain the pure phases (see Figure S1).

Single Crystal X-ray Diffraction. For $Li_6(Mo_2O_5)_3(SeO_3)_6$, a colorless rod-shaped crystal ($0.10 \times 0.01 \times 0.01$ mm^3); for $Li_2(MoO_3)(TeO_3)$, a colorless block crystal ($0.40 \times 0.20 \times 0.20$ mm^3); for $Li_2(WO_3)(TeO_3)$, a colorless block crystal ($0.04 \times 0.04 \times 0.02$ mm^3) were used for single-crystal X-ray data collections. Data were collected using a Siemens SMART APEX diffractometer equipped with a 1K CCD area detector using graphite-monochromated Mo Kα radiation. A hemisphere of data was collected using a narrow-frame method with scan widths of 0.30° in ω and an exposure time of 45 s per frame. The first 50 frames were remeasured at the end of the data collection to monitor instrument and crystal stability. The data were integrated using the Siemens SAINT program,[65] with the intensities corrected for Lorentz, polarization, air absorption, and absorption attributable to the variation in the path length through the detector face plate. Psi-scans were used for the absorption correction on the hemisphere of data.[66] The data were solved and refined using SHELXS-97 and SHELXL-97, respectively.[67,68] All of the atoms were refined with anisotropic thermal parameters, and the refinement converged for $I > 2\sigma(I)$. All calculations were performed using the WinGX-98 crystallographic software package.[69] The Flack parameter[70] for $Li_6(Mo_2O_5)_3(SeO_3)_6$ was refined to 0.000(8). Crystallographic data and selected bond distances for $Li_6(Mo_2O_5)_3(SeO_3)_6$, $Li_2(MoO_3)(TeO_3)$, and $Li_2(WO_3)(TeO_3)$ are given in Tables 1−3.

Table 1. Crystallographic Data for $Li_6(Mo_2O_5)_3(SeO_3)_6$, $Li_2(MoO_3)(TeO_3)$, and $Li_2(WO_3)(TeO_3)$

formula	$Li_6(Mo_2O_5)_3(SeO_3)_6$	$Li_2(MoO_3)(TeO_3)$	$Li_2(WO_3)(TeO_3)$
fw (g/mol)	1619.04	333.42	421.33
T (K)	298.0(2)	298.0(2)	298.0(2)
λ (Å)	0.71073	0.71073	0.71073
crystal system	orthorhombic	monoclinic	monoclinic
space group	$Pmn2_1$ (No.31)	$P2_1/n$ (No.14)	$P2_1/n$ (No.14)
a (Å)	8.2687(4)	5.3830(5)	5.3950(5)
b (Å)	16.6546(7)	13.0027(11)	12.9440(12)
c (Å)	19.2321(8)	6.9814(6)	7.0149(7)
α	90	90	90
β	90	94.7420(10)	94.2510(10)
γ	90	90	90
V (Å^3)	2648.5(2)	486.97(7)	488.52(8)
Z	4	4	4
ρ_{calcd} (g/cm^3)	4.060	4.548	5.729
μ (mm^{-1})	11.138	8.509	29.443
$2\theta_{max}$ (deg)	53.8	57.8	58.3
R (int)	0.0516	0.0620	0.0441
GOF (F^2)	0.992	1.169	1.197
R (F)[a]	0.0282	0.0282	0.0209
$R_w(F_o^2)$[b]	0.0633	0.0709	0.0528
Flack param.	0.000(8)	-	-

[a] $R(F) = \Sigma||F_o| - |F_c||/\Sigma|F_o|$. [b] $R_w(F_o^2) = [\Sigma w(F_o^2 - F_c^2)^2/\Sigma w(F_o^2)^2]^{1/2}$.

Powder X-ray Diffraction. The X-ray powder diffraction data for all compounds were collected in continuous mode using a PANalytical X'Pert PRO diffractometer at room temperature (Cu Kα radiation, flat plate geometry) equipped with X'Celerator detector. Data were collected in the 2θ range of 5−70° with a step size of 0.008° and a step time of 0.3s.

Infrared (IR) Spectroscopy. Infrared spectra were recorded on a Matteson FTIR 5000 spectrometer in the spectral range of 400−4000 cm^{-1} at room temperature. The sample (~5 mg) was finely ground with dry KBr (~100 mg). This powder mixture was then transferred to a stainless steel IR holder and pressed to a semitransparent pellet that was used for IR collection.

UV−Vis Diffuse Reflectance Spectroscopy. UV−vis diffuse reflectance spectra were collected with a Varian Cary 500 scan UV−vis−NIR spectrophotometer over the spectral range of 200−2000 nm at room temperature. Polytetrafluoroethylene (PTFE) was used as a standard material for the baseline correction. The sample was thoroughly mixed with PTFE, and this mixture was used for UV−vis measurements. Reflectance spectra were converted to absorbance using the Kubelka−Munk equation.[71,72]

Thermal Analysis. Thermogravimetric and differential thermal analyses were simultaneously carried out on an EXSTAR6000 TG/DTA 6300 Thermogravimetric/Differential Thermal Analysis system (SII NanoTechnology Inc.). The sample (~20 mg) was placed in a platinum crucible that was heated (cooled) at a rate of 10 °C/min in the range of 25−700 °C under flowing nitrogen gas. An empty platinum crucible was used as the reference during the measurements.

Second Harmonic Generation. Powder SHG measurements on $Li_6(Mo_2O_5)_3(SeO_3)_6$ were performed at room temperature on a modified Kurtz-NLO system,[73] using a pulsed Nd:YAG laser with a wavelength of 1064 nm. The methodology and instrumentation details have been published.[74] The SHG efficiency has been shown to be particle size dependent.[73] Thus, the polycrystalline samples were ground and sieved into distinct particle size ranges (20−45, 45−63, 63−75, 75−90, and 90−120 μm). In order to evaluate relative SHG efficiencies of the measured samples with known SHG materials crystalline α-SiO_2 was

dx.doi.org/10.1021/ic301334c | Inorg. Chem. 2012, 51, 9529−9538

Table 2. Selected Bond Distances (Å) for $Li_6(Mo_2O_5)_3(SeO_3)_6$

$Li_6(Mo_2O_5)_3(SeO_3)_6$					
Mo(1)−O(1)	1.684(6)	Mo(4)−O(30)	2.173(6)	Se(3)−O(22)	1.724(7)
Mo(1)−O(2)	1.709(6)	Mo(4)−O(33)	1.964(4)	Se(3)−O(23)	1.707(5)
Mo(1)−O(3)	1.953(4)	Mo(4)−O(36)	1.691(6)	Se(4)−O(16)x2	1.757(5)
Mo(1)−O(4)	1.971(5)	Mo(4)−O(39)	1.709(6)	Se(4)−O(17)	1.642(8)
Mo(1)−O(5)	2.187(6)	Mo(5)−O(11)	1.942(4)	Se(5)−O(6)	1.710(7)
Mo(1)−O(6)	2.303(5)	Mo(5)−O(15)	2.214(6)	Se(5)−O(7)	1.713(5)
Mo(2)−O(8)	1.950(4)	Mo(5)−O(27)	1.960(6)	Se(6)−O(10)x2	1.750(6)
Mo(2)−O(10)	1.989(6)	Mo(5)−O(32)	1.702(6)	Se(6)−O(14)	1.637(8)
Mo(2)−O(23)	2.216(5)	Mo(5)−O(37)	2.294(5)	Se(7)−O(28)x2	1.696(5)
Mo(2)−O(24)	1.697(6)	Mo(5)−O(40)	1.712(6)	Se(7)−O(35)	1.703(9)
Mo(2)−O(26)	2.285(6)	Mo(6)−O(19)	1.974(5)	Se(8)−O(30)	1.694(6)
Mo(2)−O(29)	1.698(5)	Mo(6)−O(22)	2.281(5)	Se(8)−O(37)	1.702(8)
Mo(3)−O(7)	2.164(5)	Mo(6)−O(25)	1.958(4)	Se(9)−O(15)x2	1.704(5)
Mo(3)−O(16)	1.977(6)	Mo(6)−O(28)	2.229(5)	Se(9)−O(26)	1.704(9)
Mo(3)−O(20)	1.951(4)	Mo(6)−O(34)	1.686(6)	Se(10)−O(5)x2	1.714(6)
Mo(3)−O(31)	1.706(6)	Mo(6)−O(41)	1.706(6)	Se(10)−O(9)	1.692(8)
Mo(3)−O(35)	2.301(6)	Se(1)−O(13)	1.639(9)	Se(11)−O(12)	1.635(9)
Mo(3)−O(38)	1.715(6)	Se(1)−O(19)x2	1.753(5)	Se(11)−O(18)x2	1.744(6)
Mo(4)−O(9)	2.272(6)	Se(2)−O(4)x2	1.745(6)	Se(12)−O(27)x2	1.757(5)
Mo(4)−O(18)	1.982(6)	Se(2)−O(21)	1.629(8)	Se(12)−O(42)	1.630(9)

Table 3. Selected Bond Distances (Å) for $Li_2(MoO_3)(TeO_3)$ and $Li_2(WO_3)(TeO_3)$

$Li_2(MoO_3)(TeO_3)$		$Li_2(WO_3)(TeO_3)$	
Mo−O(1)	1.733(3)	W−O(1)	1.755(4)
Mo−O(2)	1.740(3)	W−O(2)	1.759(4)
Mo−O(3)	1.768(3)	W−O(3)	1.796(3)
Mo−O(4)	2.124(3)	W−O(4)	2.091(4)
Mo−O(5)	2.151(3)	W−O(5)	2.122(4)
Mo−O(6)	2.369(3)	W−O(6)	2.314(4)
Te−O(4)	1.920(3)	Te−O(4)	1.929(4)
Te−O(5)	1.899(3)	Te−O(5)	1.913(3)
Te−O(6)	1.869(3)	Te−O(6)	1.878(4)

also ground and sieved into the same particle size ranges. No index matching fluid was used in the experiments.

Piezoelectric Measurements. Converse piezoelectric measurements were performed at room temperature using a Radiant Technologies RT66A piezoelectric test system with a TREK (model 609 × 10^{-6}) high voltage amplifier, Precision Materials Analyzer, Precision High Voltage Interface, and MTI 2000 Fotonic Sensor. $Li_6(Mo_2O_5)_3(SeO_3)_6$ was pressed into a pellet (~8 mm diameter and ~1 mm thick). The pellet was sintered at 300 °C for one week. Silver paste was applied to both sides of the sintered pellet as electrodes, and the pellet was cured at 300 °C for 72 h in air. This pellet was also used in polarization measurements.

Polarization Measurements. The polarization measurements were done on a Radiant Technologies Model RT66A ferroelectric test system with a TREK high-voltage amplifier in the temperature range of 25−180 °C in a Delta Model 9023 environmental test chamber. The unclamped pyroelectric coefficient, defined as dP/dT,[74] was determined by measuring the polarization as a function of temperature. The methodology and instrumentation details have been published.[74] To measure the potential ferroelectric behavior, frequency-dependent polarization measurements were done at room temperature under static electric field of 5−10 kV/cm between 50−1000 Hz. For the pyroelectric measurements, the polarization was measured statically from room temperature to 180 °C with an electric field of 7.5 kV/cm and at 1000 Hz for $Li_6(Mo_2O_5)_3(SeO_3)_6$. The temperature was allowed to stabilize before the polarization was measured.

Electron Localization Function (ELF) Calculations. Electron localization function (ELF)[75,76] calculations were performed using the plane-wave pseudopotential method (PWPP) as implemented in the Quantum ESPRESSO (4.1.2 version)[77] package. Norm-conserving MT pseudopotentials for all the elements were used with the GGA[78] for exchange-correlation corrections. The pseudopotentials generated from the Fritz Haber Institute (FHI) code[79] were converted for the calculations. The tungsten pseudopotential was generated using previously reported parameters[80] by the LD1.x program in the Quantum ESPRESSO package.[77] A plane wave energy cutoff was set to 37 Ry (Ry). The Brillouin zone was sampled using a 8 × 6 × 7 Monkhorst−Pack (MP)[81] k-mesh. A total energy convergence threshold of 10^{-6} Ry indicated self-consistency. The experimental crystal structures were employed for all calculations. The program VESTA was used for all the structural diagrams.[82]

RESULTS AND DISCUSSION

Structures. $Li_6(Mo_2O_5)_3(SeO_3)_6$ crystallizes in the NCS polar orthorhombic space group $Pmn2_1$. Ball-and-stick and polyhedral representations of the material in the *bc*-plane are shown in Figure 1. The material exhibits zigzag layers that consist of MoO_6 octahedra and SeO_3 polyhedra (see Figure 2a). Along the *a*-axis direction, two MoO_6 octahedra share an edge to form a Mo_2O_{10} dimer. The Mo_2O_{10} dimers are connected by SeO_3 polyhedra to form a layer in the *ab*-plane. The layers stack along the *c*-axis direction and are separated by the Li^+ cations (see Figure 1). In connectivity terms, the structure may be written as $[6(MoO_{2/1}O_{3/2}O_{1/3})^{-5/3}\ 3(SeO_{2/2}O_{1/3})^{+4/3}\ 3(SeO_{1/1}O_{2/2})^{0}]^{6-}$ with charge balance maintained by six Li^+ cations. The Mo^{6+} cations are octahedrally coordinated to six oxygen atoms with two 'short' (1.684(6)−1.715(6) Å), two 'normal' (1.942(4)−1.989(6) Å) and two 'long' (2.173(6)−2.303(5) Å) Mo−O bonds. The 'short' Mo−O bonds are terminal, and as expected the Mo^{6+} displaces toward these terminal oxygen atoms, i.e., an edge, C_2-type distortion. The Se^{4+} cations are in trigonal pyramidal environments, coordinated to three oxygen atoms with Se−O bond distances that range between 1.629(8)−1.757(5) Å. The Li^+ cations are observed in four-, five-, and six-coordinate environments, bonded to oxygen atoms with Li−O bond lengths in the range of 1.91(2)−2.00(2) Å, 2.00(2)−2.08(2) Å, and 2.04(2)−2.52(2) Å, respectively. Bond valence calculations[83] for Li^+, Mo^{6+}, Se^{4+}, and O^{2-} ions resulted in values

dx.doi.org/10.1021/ic301334c | Inorg. Chem. 2012, 51, 9529−9538

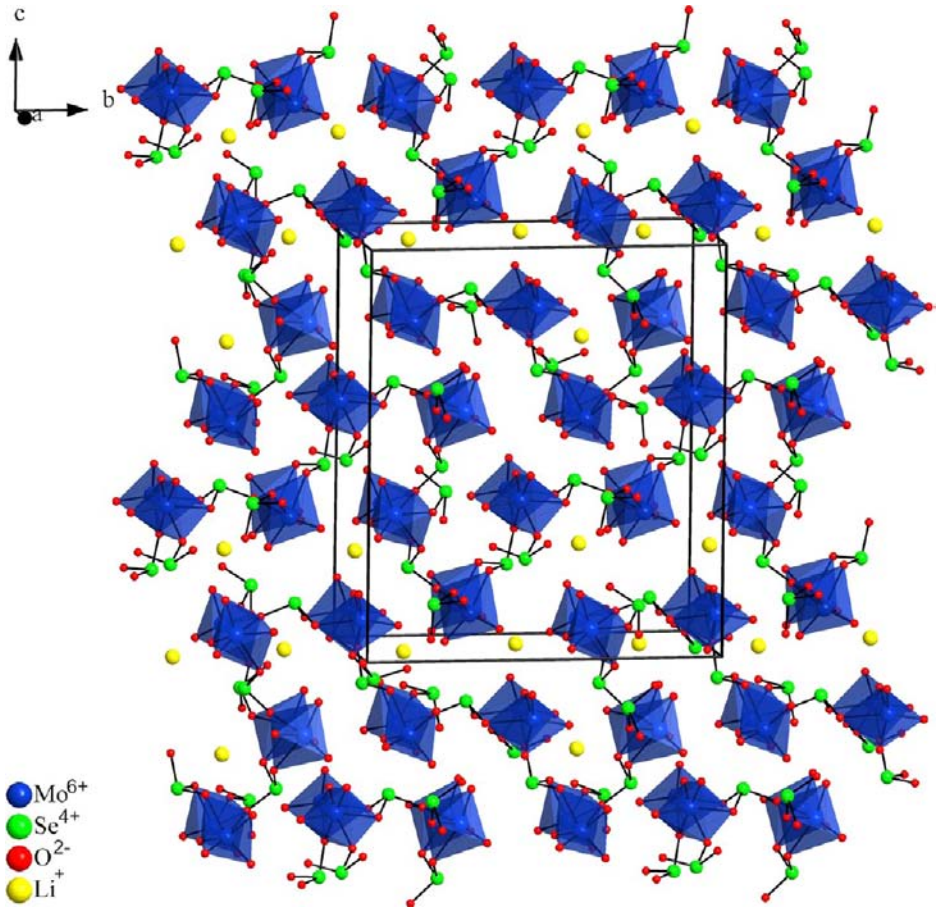

Figure 1. The polyhedra representation of $Li_6(Mo_2O_5)_3(SeO_3)_6$ in the *bc*-plane. Spheres in the diagram are Li^+ cations (yellow), Mo^{6+} cations (blue), Se^{4+} cations (green), and O^{2-} anions (red).

of 0.93−1.09, 5.96−6.07, 3.89−4.08, and 1.69−2.16, respectively (see Tables 4 and S1).

The isostructural materials, $Li_2(MoO_3)(TeO_3)$ and $Li_2(WO_3)(TeO_3)$, crystallize in the CS monoclinic space group $P2_1/n$. Ball-and-stick and polyhedral representations of $Li_2(MoO_3)(TeO_3)$ in the *bc*-plane are shown in Figure 3. Both materials also exhibit zigzag layers that consist of MO_6 octahedra and TeO_3 polyhedra (see Figure 4a). Each MO_6 (M = Mo^{6+} or W^{6+}) octahedron is connected to three TeO_3 polyhedra, and each TeO_3 polyhedron is also connected to three MO_6 octahedra to form a layer in the *ac*-plane (see Figure 4b). The layers stack along the *b*-axis direction and are separated by the Li^+ cations (see Figure 3). In connectivity terms, the structures may be written as $[(MO_{3/1}O_{3/2})^{-3}\ (TeO_{3/2})^{+}]^{2-}$ with charge balance maintained by two Li^+ cations. Mo^{6+} (W^{6+}) cations are octahedrally coordinated to six O atoms with three 'short', 1.733(3)−1.768(3)Å (1.755(4)−1.796(4) Å) and three 'long', 2.124(3)−2.369(3) Å, (2.091(4)−2.314(4) Å) M−O bonds. The 'short' M−O bonds are terminal, and as expected the M^{6+} cation displaces toward these terminal oxygen atoms, i.e., a face, C_3-type distortion. The Te^{4+} cations are in trigonal pyramidal environments, coordinated to three oxygen atoms with Te−O bond distances that range between 1.869(3)−1.920(3) Å (1.878(3)−1.929(3)Å) for $Li_2(MoO_3)(TeO_3)$ ($Li_2(WO_3)$-(TeO_3)). The Li^+ cations are observed in four- and five-coordinate environments, bonded to oxygen atoms with Li−O bond lengths in the range of 1.929(10)−2.106(10) Å and 1.964(11)−2.273(11) Å, respectively. Bond valence calculations[83] for Li^+, $Mo^{6+}(W^{6+})$, Te^{4+}, and O^{2-} ions resulted in values of 0.84−1.01, 6.00(6.00), 3.64−3.74, and 1.78−2.12, respectively (see Table 4 and S2).

Octahedral Distortion, ELF, Dipole Moments, BSI and GII Calculations. As mentioned earlier, $Li_6(Mo_2O_5)_3(SeO_3)_6$ and $Li_2(MO_3)(TeO_3)$ (M = Mo^{6+} or W^{6+}) contain SOJT distorted cations, i.e. octahedrally coordinated d^0 transition metal cations, Mo^{6+} and W^{6+}, and lone-pair cations, Se^{4+} and Te^{4+}. We are able to quantify the magnitude of the displacement of the M^{6+} cations by using the SHAPE program.[84] In the reported materials, the displacement magnitude is approximately 0.11−0.13 $Å^2$ (see Table 5). These values are consistent with those reported for Mo^{6+} and W^{6+} cations.[85]

With the lone-pair cations, ELF calculations were performed. As seen in Figure 5, violet lobe-like ELF iso-surfaces (η = 0.9) above the SeO_3 and TeO_3 polyhedra are consistent with a stereoactive lone-pair. In order to quantitatively examine the polarization magnitudes and directions of the MO_6 and AO_3 polyhedra, the dipole moments were calculated using a method described earlier[21] and extended subsequently for lone-pair cations.[86] The calculated dipole moments for the MoO_6, WO_6, SeO_3, and TeO_3 polyhedra are 4.4−6.9D, 2.8D, 7.9−9.5D, and 13.1−13.5D, respectively. These values are consistent with those reported earlier.[44,87] The smaller dipole moment for the WO_6 octahedron is reasonable since in the method used, the magnitude of the dipole moment is inversely proportional to the atomic number. The approximate direction of the dipole moments of the MoO_6, WO_6, SeO_3, and TeO_3 polyhedra are

dx.doi.org/10.1021/ic301334c | Inorg. Chem. 2012, 51, 9529−9538

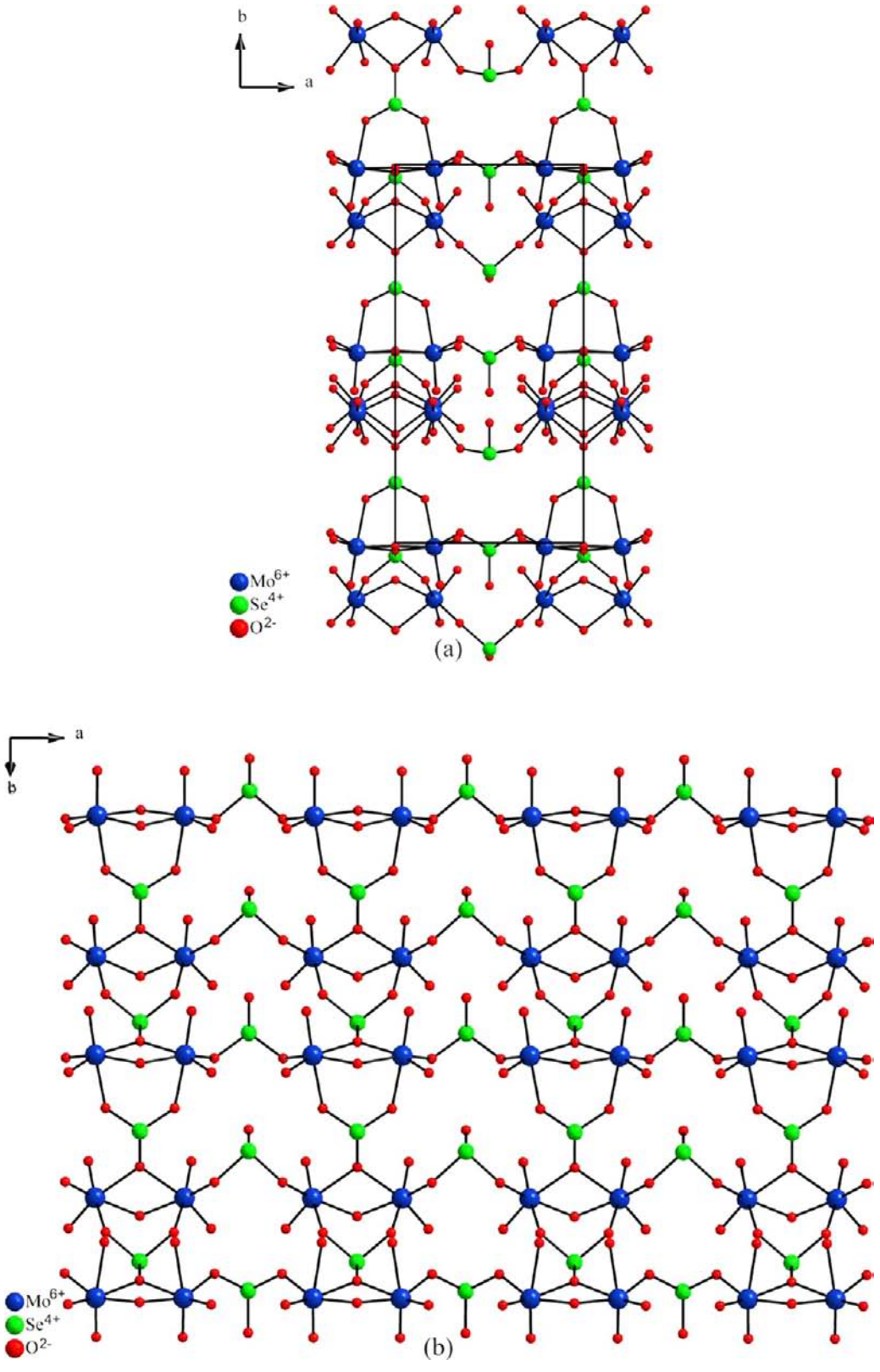

Figure 2. Ball-and-stick representations of $[6(MoO_{2/1}O_{3/2}O_{1/3})^{-5/3}\ 3(SeO_{2/2}O_{1/3})^{+4/3}\ 3(SeO_{1/1}O_{2/2})^{0}]^{6-}$ zigzag layers in the *ab*-plane (top) and connectivity between Mo_2O_{10} dimers and SeO_3 polyhedra in the layer section (bottom). Spheres in the diagram are Mo^{6+} cations (blue), Se^{4+} cations (green), and O^{2-} anions (red). The Li^+ cations have been removed for clarity.

shown in Figure 5. With $Li_2(MO_3)(TeO_3)$ (M = Mo^{6+} or W^{6+}), the MO_6 and TeO_3 polyhedra in two adjacent $[(MO_{3/1}O_{3/2})^{-3}(TeO_{3/2})^{+}]^{2-}$ layers are oriented in an antiparallel manner that results in complete cancelation of the individual dipole moments. Whereas for $Li_6(Mo_2O_5)_3(SeO_3)_6$, the dipole moments of the MoO_6 and SeO_3 polyhedra are partly aligned along *c*-axis - consistent with the polar axis direction of the crystal class, *mm2*.[88] However, as $Li_6(Mo_2O_5)_3(SeO_3)_6$ has a zigzag layer topology

dx.doi.org/10.1021/ic301334c | *Inorg. Chem.* 2012, 51, 9529−9538

Table 4. Bond Valence Sum (vu), Bond Strain Index (BSI), and Global Instability Index (GII) of $Li_6(Mo_2O_5)_3(SeO_3)_6$ and $Li_2(MO_3)(TeO_3)$ (M = Mo^{6+} or W^{6+})[a]

	bond valence sum					functional properties			
compound	Li^+	M^{6+}	A^{4+}	BSI	GII	SHG	d_{33}	P_T	P_m
$Li_6(Mo_2O_5)_3(SeO_3)_6$	0.93−1.09	5.96−6.07	3.89−4.08	0.12	0.09	170	28	−0.43	0.05
$Li_2(MoO_3)(TeO_3)$	0.86−1.01	6.00	3.74	0.11	0.14				
$Li_2(WO_3)(TeO_3)$	0.84−1.00	6.00	3.64	0.11	0.17				

[a]SHG efficiency (× α-SiO_2), piezoelectric response, d_{33} (pm/V), pyroelectric coefficient, P_T ($\mu C/m^2K$), and maximum polarization, P_m ($\mu C/m^2$) for $Li_6(Mo_2O_5)_3(SeO_3)_6$ are also given.

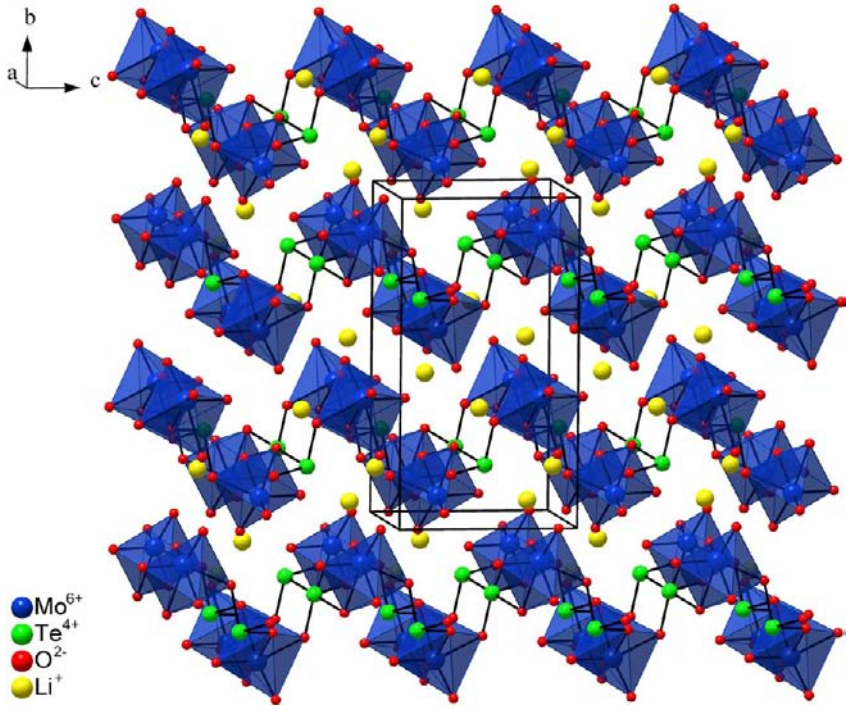

Figure 3. The polyhedra representation of $Li_2(MoO_3)(TeO_3)$ in the *bc*-plane. Spheres in the diagram are Li^+ cations (yellow), Mo^{6+} cations (blue), Te^{4+} cations (green), and O^{2-} anions (red).

(see Figure 1), the dipole moments of the MoO_6 and SeO_3 polyhedra do not fully 'constructively add', and only a small dipole moment of 3.7 D per unit cell is observed.

In order to better understand the influence of the polar MO_6 and AO_3 polyhedra on the structures of the reported materials, bond strain and global instability indices, BSI and GII respectively, were calculated.[83,89,90] The BSI and GII indices are indicative of electronic- and lattice-induced strains, respectively. Values greater than 0.05 vu (valence units) indicate the structures are strained. For the reported materials, the BSI and GII values are greater than 0.05 vu (see Table 4). This is not surprising given the occurrence of asymmetric polyhedra. As seen in Table 4, the BSI values are very similar, i.e., 0.11−0.12 vu. The BSI is attributable to electronic, or SOJT, distortions, and as the reported materials have similar SOJT distorted cations it is reasonable to expect the BSI values to be similar. The GII indices increase from $Li_6(Mo_2O_5)_3(SeO_3)_6$ (0.09 vu) to $Li_2(MoO_3)$-(TeO_3) (0.14 vu) and $Li_2(WO_3)(TeO_3)$ (0.17 vu). With BSI > GII, as is the situation with $Li_6(Mo_2O_5)_3(SeO_3)_6$, the structural strains are electronically induced, i.e., the bond distances of the SOJT distorted cations are mainly determined by electronic distortions. With BSI < GII, as is the case for $Li_2(MoO_3)(TeO_3)$ and $Li_2(WO_3)(TeO_3)$, the structural strains are lattice-induced, i.e., the bond distances of the SOJT distorted cations − specifically Te^{4+} − are impacted greatly by the surrounding polyhedra. The average Te−O bond distances in $Li_2(MoO_3)(TeO_3)$ and $Li_2(WO_3)(TeO_3)$ are 1.896 Å and 1.907 Å, respectively, longer than what is usually observed.[34,64] As such, the bond valence sums for the Te^{4+} cations in these materials are reduced and the GII increases.

IR Spectroscopy. The IR spectra for $Li_6(Mo_2O_5)_3(SeO_3)_6$ and $Li_2(MO_3)(TeO_3)$ (M = Mo^{6+} or W^{6+}) showed no absorption bands in the IR region of 4000−1000 cm^{-1}. Both spectra revealed absorption bands of Mo(W)−O, Se(Te)−O vibrations in the 400−1000 cm^{-1} range. The Mo(W)−O stretching vibrations were observed around 811−940 cm^{-1}, whereas Se(Te)−O stretching vibrations were seen around 673−750 cm^{-1}. The absorption band occurring below 650 cm^{-1} can be assigned to Mo(W)−O−Se(Te) bending vibrations. These assignments are in good agreement with the literature.[91−93] The IR spectra and assignments were deposited in the Supporting Information (see Figure S2).

UV−Vis Diffuse Reflectance Spectroscopy. Reflectance spectra of $Li_6(Mo_2O_5)_3(SeO_3)_6$ and $Li_2(MO_3)(TeO_3)$ (M = Mo^{6+} or W^{6+}) were converted to absorbance using the Kubelka−Munk function[71,72]

$$F(R) = (1 - R)^2/2R = K/S$$

dx.doi.org/10.1021/ic301334c | Inorg. Chem. 2012, 51, 9529−9538

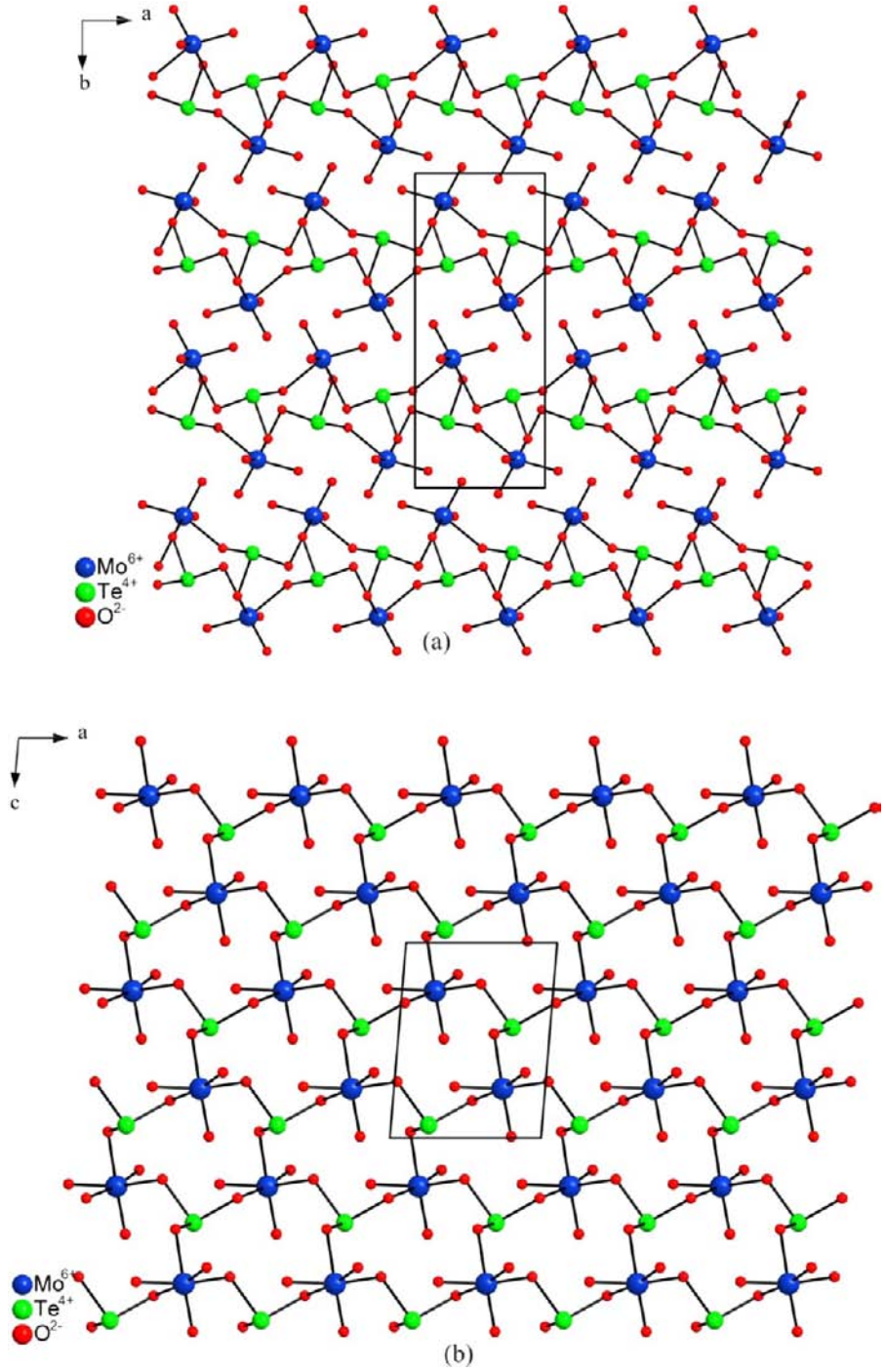

Figure 4. Ball-and-stick representations of $[(MO_3O_{3/2})^{-3}\ (TeO_{3/2})^{+1}]^{2-}$ zigzag layers in the *ab*-plane (top) and connectivity between MoO_6 and TeO_3 polyhedra in the layer (bottom). Spheres in the diagram are Mo^{6+} cations (blue), Te^{4+} cations (green), and O^{2-} anions (red). The Li^+ cations have been removed for clarity.

where R, K, and S represent the reflectance, the absorption, and the scattering, respectively. In a F(R) versus E (eV) plot, extrapolating the linear part of the rising curve to zero provides onset absorption of 3.3 eV, 3.5 eV, and 4.0 eV for $Li_6(Mo_2O_5)_3(SeO_3)_6$, $Li_2(MoO_3)(TeO_3)$, and $Li_2(WO_3)(TeO_3)$, respectively. These values are consistent with the transparency of the materials in the visible wavelength. The UV−vis diffuse reflectance spectra for the reported compounds were deposited in the Supporting Information (see Figure S3).

Thermal Analysis. The thermal stability of $Li_6(Mo_2O_5)_3(SeO_3)_6$, $Li_2(MoO_3)(TeO_3)$, and $Li_2(WO_3)(TeO_3)$ were investigated through thermogravimetric and differential thermal analyses (TGA and DTA). The TGA and DTA data of $Li_6(Mo_2O_5)_3(SeO_3)_6$ indicated that the material releases SeO_2 at ~460 °C and decomposes to $Li_4Mo_5O_{17}$. The experimental weight loss (41.4%) indicated $Li_6(Mo_2O_5)_3(SeO_3)_6$ releases six SeO_2 equivalents during its thermal decomposition (calculated weight loss of 41.0%). The endothermic peak at ~520 °C on the heating curve and the exothermic peak at ~450 °C on the cooling curve of $Li_6(Mo_2O_5)_3(SeO_3)_6$ are attributable to the melting and cooling processes of a congruent melting oxide, $Li_4Mo_5O_{17}$.[94] For $Li_2(MoO_3)(TeO_3)$, the heating curve showed a large

dx.doi.org/10.1021/ic301334c | *Inorg. Chem.* 2012, 51, 9529−9538

Table 5. Distortion Magnitudes of MO_6 Octahedra, Dipole Moments of MO_6 (M = Mo^{6+} or W^{6+}), and AO_3 (A = Se^{4+} or Te^{4+}) Polyhedra in $Li_6(Mo_2O_5)_3(SeO_3)_6$ and $Li_2(MO_3)(TeO_3)$

compounds		polyhedral dipole moment (D)					MO_6 distortion magnitude ($Å^2$)
$Li_6(Mo_2O_5)_3(SeO_3)_6$	$Mo(1)O_6$	5.7	$Se(1)O_3$	8.1	$Se(7)O_3$	9.1	0.12
	$Mo(2)O_6$	5.1	$Se(2)O_3$	8.6	$Se(8)O_3$	9.5	0.12
	$Mo(3)O_6$	5.1	$Se(3)O_3$	8.5	$Se(9)O_3$	8.7	0.11
	$Mo(4)O_6$	5.2	$Se(4)O_3$	7.9	$Se(10)O_3$	8.5	0.11
	$Mo(5)O_6$	5.5	$Se(5)O_3$	8.6	$Se(11)O_3$	8.4	0.12
	$Mo(6)O_6$	4.4	$Se(6)O_3$	8.2	$Se(12)O_3$	8.4	0.11
$Li_2(MoO_3)(TeO_3)$	MoO_6	6.9	TeO_3	13.5			0.13
$Li_2(WO_3)(TeO_3)$	WO_6	2.8	TeO_3	13.1			0.11

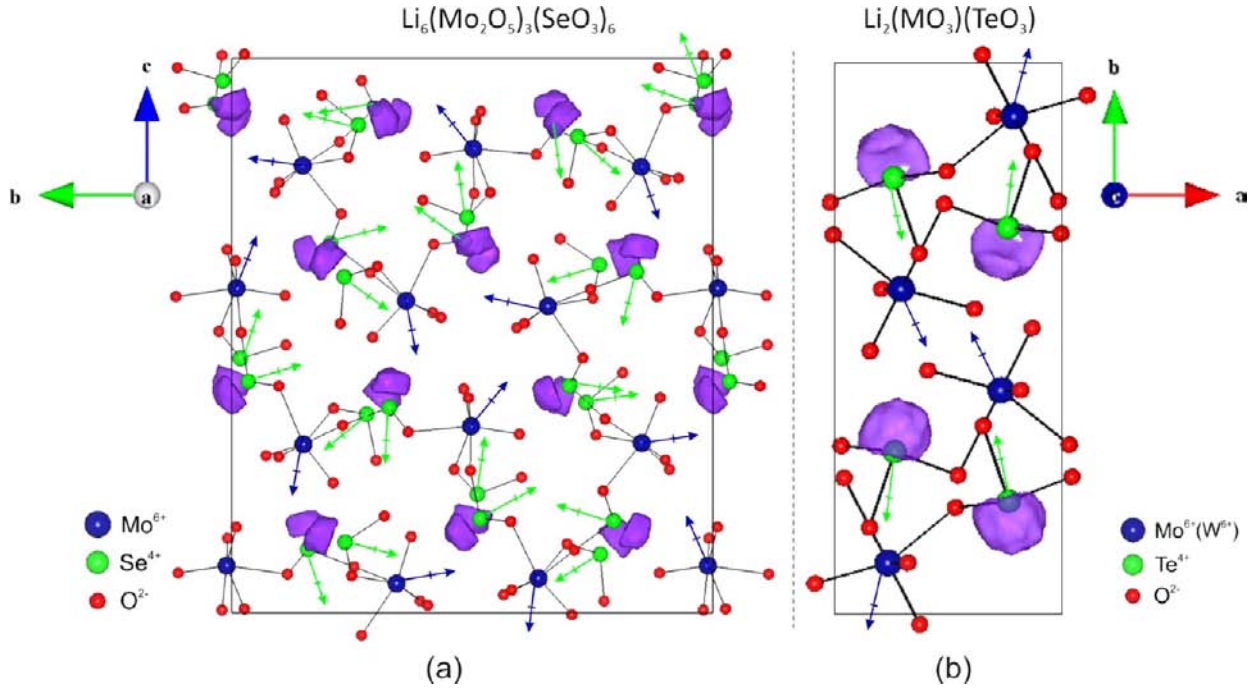

Figure 5. Ball-and-stick representations of (a) $Li_6(Mo_2O_5)_3(SeO_3)_6$ in the *bc*-plane and (b) $Li_2(MO_3)(TeO_3)$ (M = Mo^{6+} or W^{6+}) in the *ab*-plane. The arrows indicate the approximate directions of the dipole moments of the MoO_6 (blue) and AO_3 (A = Se^{4+} or Te^{4+}) (green) polyhedra in the unit cell. Electron localization function (ELF) plots with η = 0.9 is also shown. The lobe-like iso-surfaces near top of AO_3 polyhedra are consistent with a stereoactive lone-pair on the A cations. The Li^+ cations have been removed for clarity.

endothermic peak at ~470 °C indicating $Li_2(MoO_3)(TeO_3)$ had melted. For $Li_2(WO_3)(TeO_3)$, the heating curve revealed a small endothermic peak at ~485 °C and a large endothermic peak ~560 °C indicating $Li_2(WO_3)(TeO_3)$ had melted. No peak was observed on the cooling curves of both oxides, and no weight loss was found on their TGA curves up to 700 °C. The PXRD patterns of the residuals showed $Li_2(WO_3)(TeO_3)$ decomposed to Li_2WO_4, whereas $Li_2(MoO_3)(TeO_3)$ decomposed to Li_2MoO_4. The DTA and TGA data and PXRD pattern of the residuals are deposited in the Supporting Information (see Figures S4 and S5).

Second Harmonic Generation. Powder SHG measurements on $Li_6(Mo_2O_5)_3(SeO_3)_6$ indicated the material has an SHG efficiency of approximately 170 × α-SiO_2 in the particle size range of 45−63 μm. The SHG efficiency as a function of particle size was measured, in the particle size range of 25−120 μm. The measurements indicated that $Li_6(Mo_2O_5)_3(SeO_3)_6$ is type 1 nonphase matching. $Li_6(Mo_2O_5)_3(SeO_3)_6$ falls into the class C of SHG materials as defined by Kurtz and Perry.[73] The average NLO susceptibility,[74] $\langle d_{eff}\rangle_{exp}$, can be estimated to be approximately 9.8 pm/V, compared to recently reported SHG efficiency of $Ba(Mo_2O_5)(SeO_3)_2$ (10.3 pm/V).[9] The moderate SHG is attributable to the net polarization − the partial addition of the MoO_6 and SeO_3 dipole moments. As mentioned earlier, the alignment of their dipole moments along the *c*-axis direction gives rise to the net dipole moment of 3.7 D per unit cell. That net dipole moment contributes not only to the SHG efficiency of $Li_6(Mo_2O_5)_3(SeO_3)_6$ but also to its pyroelectric behavior. The power SHG data have been deposited in the Supporting Information (see Figure S6).

Piezoelectricity Measurements. Converse piezoelectric measurements were performed on $Li_6(Mo_2O_5)_3(SeO_3)_6$ pellet at room temperature. A voltage of 750 V at 200 Hz was applied for $Li_6(Mo_2O_5)_3(SeO_3)_6$. The d_{33} piezoelectric charge constants,[74] which is defined as the ratio between the strain produced and the electrical voltage applied, for $Li_6(Mo_2O_5)_3(SeO_3)_6$ was estimated to be 28 pm/V. This charge constant is comparable to $Zn_2(MoO_4)(SeO_3)$ (d_{33} = 14 pm/V).[95] The piezoelectric data were deposited in the Supporting Information (see Figure S7).

Polarization Measurements. $Li_6(Mo_2O_5)_3(SeO_3)_6$ is not only NCS but also polar − a macroscopic dipole moment is observed. The macroscopic polarity suggests the possibility for ferroelectric behavior. Ferroelectric hysteresis measurements

dx.doi.org/10.1021/ic301334c | Inorg. Chem. 2012, 51, 9529−9538

were performed on pressed pellets, and 'polarization loops' were observed. In addition, these loops did appear to exhibit frequency dependence (see Figure S8). However, these loops are not attributable to ferroelectric hysteresis but likely attributable to dielectric loss. Thus the reported materials are not ferroelectric – the macroscopic polarization cannot be reversed in the presence of an external electric field. It has been demonstrated that these types of loops have been erroneously attributed to ferroelectric behavior.[96] With the reported materials, it is important to understand why the materials, although polar, are not ferroelectric. As stated earlier, for ferroelectric behavior to occur the macroscopic polarization must be switchable or reversible in the presence of an external electric field. This implies that the local moments must also be reversed. In $Li_6(Mo_2O_5)_3(SeO_3)_6$ only the SeO_3 and MoO_6 polyhedra exhibit a local dipole moment. Thus it is these dipole moments that must be reversed for ferroelectric behavior to occur. We have already shown that the energy barrier to inversion a SeO_3 trigonal-pyramid is ~5.3 eV,[40] which is substantially larger than what is observed in ferroelectric $BaTiO_3$ (1.8×10^{-2} eV) and $PbTiO_3$ (2.0×10^{-1} eV).[97] Thus it is energetically unfavorable for polarization reversal to occur. Therefore, $Li_6(Mo_2O_5)_3(SeO_3)_6$ is pyroelectric and not ferroelectric.

Pyroelectric measurements were performed by measuring the polarization (P) as a function of temperature. The value of the pyroelectric coefficient, which is defined as dP/dT,[74] for $Li_6(Mo_2O_5)_3(SeO_3)_6$ at 50 °C is $-0.43\ \mu C/m^2K$. The polarization data were deposited in the Supporting Information (see Figure S8).

CONCLUSION

New quaternary lithium – d^0 cation – lone-pair oxides, NCS polar $Li_6(Mo_2O_5)_3(SeO_3)_6$ ($Pmn2_1$) and CS $Li_2(MO_3)(TeO_3)$ ($P2_1/n$) (M = Mo^{6+} or W^{6+}), have been synthesized and characterized. The oxides exhibit a layered structure with distorted MO_6 (M = Mo^{6+} or W^{6+}) and asymmetric AO_3 (A = Se^{4+} or Te^{4+}) polyhedra. $Li_6(Mo_2O_5)_3(SeO_3)_6$ exhibits a SHG efficiency of 170 × α-SiO_2 and is type 1 nonphase-matchable. Although $Li_6(Mo_2O_5)_3(SeO_3)_6$ is polar, the macroscopic polarization is not reversible, and the material is not ferroelectric.

ASSOCIATED CONTENT

Supporting Information

X-ray crystallographic files in CIF format, experimental and calculated powder X-ray diffraction patterns, infrared and UV–vis spectra, thermogravimetric and differential thermal analysis diagrams, bond analyses for $Li_6(Mo_2O_5)_3(SeO_3)_6$ and $Li_2(MO_3)(TeO_3)$ (M = Mo^{6+} or W^{6+}), SHG behaviors, piezoelectric and polarization-electric loops for $Li_6(Mo_2O_5)_3(SeO_3)_6$. This material is available free of charge via the Internet at http://pubs.acs.org.

AUTHOR INFORMATION

Corresponding Author

*E-mail: psh@uh.edu.

Notes

The authors declare no competing financial interest.

ACKNOWLEDGMENTS

We thank the Robert A. Welch Foundation (Grant E-1457) for support. Sau Nguyen thanks the Vietnam Government for an opportunity to study at the University of Houston.

REFERENCES

(1) Jaffe, B.; Cook, W. R.; Jaffe, H. *Piezoelectric ceramics*; Academic Press: 1971.
(2) Jona, F.; Shirane, G. *Ferroelectric Crystals*; Pergamon Press: 1961.
(3) Lang, S. B.; Das-Gupta, D. K. Academic Press: 2001; Vol. *4*, p 1.
(4) Munn, R. W.; Ironside, C. N. *Principles and Applications of Nonlinear Optical Materials*; Blackie Academic & Professional: Glasgow, 1993.
(5) Marvel, M. R.; Lesage, J.; Baek, J.; Halasyamani, P. S.; Stern, C. L.; Poeppelmeier, K. R. *J. Am. Chem. Soc.* **2007**, *129*, 13963.
(6) Chang, H.-Y.; Kim, S.-H.; Ok, K. M.; Halasyamani, P. S. *J. Am. Chem. Soc.* **2009**, *131*, 6865.
(7) Porter, Y.; Halasyamani, P. S. *J. Solid State Chem.* **2003**, *174*, 441.
(8) Yeon, J.; Kim, S.-H.; Hayward, M. A.; Halasyamani, P. S. *Inorg. Chem.* **2011**, *50*, 8663.
(9) Oh, S.-J.; Lee, D. W.; Ok, K. M. *Inorg. Chem.* **2012**, *51*, 5393.
(10) Donakowski, M. D.; Gautier, R.; Yeon, J.; Moore, D. T.; Nino, J. C.; Halasyamani, P. S.; Poeppelmeier, K. R. *J. Am. Chem. Soc.* **2012**, *134*, 7679.
(11) Fry, A. M.; Seibel, H. A.; Lokuhewa, I. N.; Woodward, P. M. *J. Am. Chem. Soc.* **2011**, *134*, 2621.
(12) Chen, C. T. *Acta Phys. Sin.* **1976**, *25*, 146.
(13) Chen, C. T. *Acta Phys. Sin.* **1977**, *26*, 124.
(14) Chen, C. T. *Acta Phys. Sin.* **1979**, *22*, 756.
(15) Chen, C.; Wu, Y.; Li, R. *Int. Rev. Phys. Chem.* **1989**, *8*, 65.
(16) Zou, G.; Ye, N.; Huang, L.; Lin, X. *J. Am. Chem. Soc.* **2011**, *133*, 20001.
(17) Heier, K. R.; Norquist, A. J.; Halasyamani, P. S.; Duarte, A.; Stern, C. L.; Poeppelmeier, K. R. *Inorg. Chem.* **1999**, *38*, 762.
(18) Welk, M. E.; Norquist, A. J.; Stern, C. L.; Poeppelmeier, K. R. *Inorg. Chem.* **2000**, *39*, 3946.
(19) Welk, M. E.; Norquist, A. J.; Stern, C. L.; Poeppelmeier, K. R. *Inorg. Chem.* **2001**, *40*, 5479.
(20) Welk, M. E.; Norquist, A. J.; Arnold, F. P.; Stern, C. L.; Poeppelmeier, K. R. *Inorg. Chem.* **2002**, *41*, 5119.
(21) Maggard, P. A.; Nault, T. S.; Stern, C. L.; Poeppelmeier, K. R. *J. Solid State Chem.* **2003**, *175*, 27.
(22) Izumi, H. K.; Kirsch, J. E.; Stern, C. L.; Poeppelmeier, K. R. *Inorg. Chem.* **2005**, *44*, 884.
(23) Marvel, M. R.; Pinlac, R. A. F.; Lesage, J.; Stern, C. L.; Poeppelmeier, K. R. *Z. Anorg. Allg. Chem.* **2009**, *635*, 869.
(24) Bader, R. F. W. *Mol. Phys.* **1960**, *3*, 137.
(25) Bader, R. F. W. *Can. J. Chem.* **1962**, *40*, 1164.
(26) Goodenough, J. B. *Annu. Rev. Mater. Sci.* **1998**, *28*, 1.
(27) Kunz, M.; Brown, I. D. *J. Solid State Chem.* **1995**, *115*, 395.
(28) Opik, U.; Pryce, M. H. L. *Proc. R. Soc. London, Ser. A* **1957**, *238*, 425.
(29) Pearson, R. G. *J. Am. Chem. Soc.* **1969**, *91*, 4947.
(30) Pearson, R. G. *J. Mol. Struct.:THEOCHEM* **1983**, *103*, 25.
(31) Halasyamani, P. S.; Poeppelmeier, K. R. *Chem. Mater.* **1998**, *10*, 2753.
(32) Goodey, J.; Broussard, J.; Halasyamani, P. S. *Chem. Mater.* **2002**, *14*, 3174.
(33) Ra, H.-S.; Ok, K. M.; Halasyamani, P. S. *J. Am. Chem. Soc.* **2003**, *125*, 7764.
(34) Goodey, J.; Ok, K. M.; Broussard, J.; Hofmann, C.; Escobedo, F. V.; Halasyamani, P. S. *J. Solid State Chem.* **2003**, *175*, 3.
(35) Ok, K. M.; Halasyamani, P. S. *Angew. Chem., Int. Ed.* **2004**, *43*, 5489.
(36) Chi, E. O.; Ok, K. M.; Porter, Y.; Halasyamani, P. S. *Chem. Mater.* **2006**, *18*, 2070.
(37) Kim, J.-H.; Baek, J.; Halasyamani, P. S. *Chem. Mater.* **2007**, *19*, 5637.
(38) Sivakumar, T.; Chang, H. Y.; Baek, J.; Halasyamani, P. S. *Chem. Mater.* **2007**, *19*, 4710.
(39) Chang, H. Y.; Sivakumar, T.; Ok, K. M.; Halasyamani, P. S. *Inorg. Chem.* **2008**, *47*, 8511.
(40) Kim, S.-H.; Yeon, J.; Halasyamani, P. S. *Chem. Mater.* **2009**, *21*, 5335.

(41) Chang, H. Y.; Kim, S.-H.; Ok, K. M.; Halasyamani, P. S. *Chem. Mater.* **2009**, *21*, 1654.
(42) Chang, H.-Y.; Kim, S.-H.; Halasyamani, P. S.; Ok, K. M. *J. Am. Chem. Soc.* **2009**, *131*, 2426.
(43) Yeon, J.; Kim, S.-H.; Halasyamani, P. S. *Inorg. Chem.* **2010**, *49*, 6986.
(44) Chang, H. Y.; Kim, S. W.; Halasyamani, P. S. *Chem. Mater.* **2010**, *22*, 3241.
(45) Kong, F.; Huang, S.-P.; Sun, Z.-M.; Mao, J.-G.; Cheng, W.-D. *J. Am. Chem. Soc.* **2006**, *128*, 7750.
(46) Jiang, H.-L.; Xie, Z.; Mao, J.-G. *Inorg. Chem.* **2007**, *46*, 6495.
(47) Jiang, H.-L.; Huang, S.-P.; Fan, Y.; Mao, J.-G.; Cheng, W.-D. *Chem.—Eur. J.* **2008**, *14*, 1972.
(48) Zhang, S.-Y.; Jiang, H.-L.; Sun, C.-F.; Mao, J.-G. *Inorg. Chem.* **2009**, *48*, 11809.
(49) Sun, C.-F.; Hu, C.-L.; Xu, X.; Ling, J.-B.; Hu, T.; Kong, F.; Long, X.-F.; Mao, J.-G. *J. Am. Chem. Soc.* **2009**, *131*, 9486.
(50) Hu, T.; Qin, L.; Kong, F.; Zhou, Y.; Mao, J.-G. *Inorg. Chem.* **2009**, *48*, 2193.
(51) Zhang, S.-Y.; Hu, C.-L.; Sun, C.-F.; Mao, J.-G. *Inorg. Chem.* **2010**, *49*, 11627.
(52) Li, P.-X.; Kong, F.; Hu, C.-L.; Zhao, N.; Mao, J.-G. *Inorg. Chem.* **2010**, *49*, 5943.
(53) Sun, C.-F.; Hu, C.-L.; Xu, X.; Mao, J.-G. *Inorg. Chem.* **2010**, *49*, 9581.
(54) Li, P.-X.; Hu, C.-L.; Xu, X.; Wang, R.-Y.; Sun, C.-F.; Mao, J.-G. *Inorg. Chem.* **2010**, *49*, 4599.
(55) Yang, B.-P.; Hu, C.-L.; Xu, X.; Sun, C.-F.; Zhang, J.-H.; Mao, J.-G. *Chem. Mater.* **2010**, *22*, 1545.
(56) Sun, C.-F.; Hu, C.-L.; Xu, X.; Yang, B.-P.; Mao, J.-G. *J. Am. Chem. Soc.* **2011**, *133*, 5561.
(57) Darriet, J. *Bull. Soc. Fr. Mineral. Cristallogr.* **1973**, *96*, 97.
(58) Johnston, M. G.; Harrison, W. T. A. *Acta Crystallogr., Sect. C: Cryst. Struct. Commun.* **2007**, *C63*, i57.
(59) Chen, X.; Zhang, L.; Chang, X.; Xue, H.; Zang, H.; Xiao, W.; Song, X.; Yan, H. *J. Alloys Compd.* **2007**, *428*, 54.
(60) Klevtsova, R. F.; Solodovnikov, S. F.; Glinskaya, L. A.; Alekseev, V. I.; Khalbaeva, K. M.; Khaikina, E. G. *J. Struct. Chem. (Transl. Zh. Strukt. Khim.)* **1997**, *38*, 89.
(61) Harrison, W. T. A.; Dussack, L. L.; Jacobson, A. J. *Inorg. Chem.* **1994**, *33*, 6043.
(62) Harrison, W. T. A.; Dussack, L. L.; Vogt, T.; Jacobson, A. J. *J. Solid State Chem.* **1995**, *120*, 112.
(63) Dussack, L. L.; Harrison, W. T. A.; Jacobson, A. J. *Mater. Res. Bull.* **1996**, *31*, 249.
(64) Balraj, V.; Vidyasagar, K. *Inorg. Chem.* **1998**, *37*, 4764.
(65) *SAINT, Program for Area Detector Absorption Correction, version 4.05*; Siemens Analytical X-ray Systems, Inc.: Madison, WI, 1995.
(66) North, A. C. T.; Phillips, D. C.; Mathews, F. S. *Acta Crystallogr.* **1968**, *24*, 351.
(67) Sheldrick, G. M. *SHELXL-97 - A program for crystal structure refinement*; University of Goettingen: Goettingen, 1997.
(68) Sheldrick, G. M. *SHELXS-97 - A program for automatic solution of crystal structures*; University of Goettingen: Goettingen, Germany, 1997.
(69) Farrugia, L. J. *J. Appl. Crystallogr.* **1999**, *32*, 837.
(70) Flack, H. *Acta Crystallogr.* **1983**, *39*, 876.
(71) Kubelka, P.; Munk, F. *Z. Tech. Phys.* **1931**, *12*, 593.
(72) Tauc, J. *Mater. Res. Bull.* **1970**, *5*, 721.
(73) Kurtz, S. K.; Perry, T. T. *J. Appl. Phys.* **1968**, *39*, 3798.
(74) Ok, K. M.; Chi, E. O.; Halasyamani, P. S. *Chem. Soc. Rev.* **2006**, *35*, 710.
(75) Becke, A. D.; Edgecombe, K. E. *J. Chem. Phys.* **1990**, *92*, 5397.
(76) Silvi, B.; Savin, A. *Nature* **1994**, *371*, 683.
(77) Giannozzi, P. *J. Phys: Condens. Matter.* **2009**, *21*, 395502.
(78) Perdew, J. P.; Burke, K.; Ernzerhof, M. *Phys. Rev. Lett.* **1996**, *77*, 3865.
(79) Fuchs, M.; Scheffler, M. *Comput. Phys. Commun.* **1999**, *119*, 67.
(80) Walkingshaw, A. D.; Spaldin, N. A.; Artacho, E. *Phys. Rev. B: Condens. Matter* **2004**, *70*, 165110.
(81) Monkhorst, H. J.; Pack, J. D. *Phys. Rev. B* **1976**, *13*, 5188.
(82) Momma, K.; Izumi, F. *J. Appl. Crystallogr.* **2008**, *41*, 653.
(83) Brown, I. D. *The Chemical Bond in Inorganic Chemistry: The Bond Valence Model*, 1st ed.; Oxford University Press: Oxford, 2002.
(84) Llunell, M.; Casanova, D.; Cirera, J.; Bofill, J. M.; Alemany, P.; Alvarez, S.; Pinsky, M.; Avnir, D. 1.1b ed.; University of Barcelona: Barcelona, Spain, 2003.
(85) Ok, K. M.; Halasyamani, P. S.; Casanova, D.; Llunell, M.; Alemany, P.; Alvarez, S. *Chem. Mater.* **2006**, *18*, 3176.
(86) Ok, K. M.; Halasyamani, P. S. *J. Solid State Chem.* **2006**, *179*, 1345.
(87) Chang, H. Y.; Ok, K. M.; Kim, J. H.; Halasyamani, P. S.; Stoltzfus, M.; Woodward, P. *Inorg. Chem.* **2007**, *46*, 7005.
(88) *International Tables for Crystallography, Vol. A, Space Group Symmetry*; Hahn, T., Ed.; Kluwer Academic: Dordrecht, Holland, 2006; Vol. *A*.
(89) Preiser, C.; Losel, J.; Brown, I. D.; Kunz, M.; Skowron, A. *Acta Crystallogr.* **1999**, *55*, 698.
(90) Salinas-Sanchez, A.; Garcia-Muñoz, J. L.; Rodriguez-Carvajal, J.; Saez-Puche, R.; Martinez, J. L. *J. Solid State Chem.* **1992**, *100*, 201.
(91) Frechero, M. A.; Quinzani, O. V.; Pettigrosso, R. S.; Villar, M.; Montani, R. A. *J. Non-Cryst. Solids* **2007**, *353*, 2919.
(92) Harrison, W. T. A.; Dussack, L. L.; Jacobson, A. J. *J. Solid State Chem.* **1996**, *125*, 234.
(93) Kurilenko, L. N.; Serebryakova, N. V.; Saunin, E. I.; Gromov, V. V.; Sokolova, N. P. *Russ. Chem. Bull.* **1988**, *37*, 839.
(94) Brower, W. S.; Parker, H. S.; Roth, R. S.; Waring, J. L. *J. Cryst. Growth* **1972**, *16*, 115.
(95) Nguyen, S. D.; Kim, S.-H.; Halasyamani, P. S. *Inorg. Chem.* **2011**, *50*, 5215.
(96) Scott, J. F. *J. Phys.: Condens. Matter* **2008**, *20*, 021001.
(97) Cohen, R. E. *Nature* **1992**, *358*, 136.